

Modeling near wall effects in second moment closures by elliptic relaxation

By D. Laurence¹ and P. Durbin²

The elliptic relaxation model of Durbin (1993) for modeling near-wall turbulence using second moment closures (SMC) is compared to DNS data for a channel flow at $Re_t = 395$. The agreement for second order statistics and even the terms in their balance equation is quite satisfactory, confirming that very little viscous effects (via Kolmogoroff scales) need to be added to the high Reynolds versions of SMC for near-wall-turbulence. The essential near-wall feature is thus the kinematic blocking effect that a solid wall exerts on the turbulence through the fluctuating pressure, which is best modeled by an elliptic operator. Above the transition layer, the effect of the original elliptic operator decays rapidly, and it is suggested that the log-layer is better reproduced by adding a non-homogeneous reduction of the return to isotropy, the gradient of the turbulent length scale being used as a measure of the inhomogeneity of the log-layer. The elliptic operator was quite easily applied to the non-linear Craft & Launder pressure-strain model yielding an improved distinction between the spanwise and wall normal stresses, although at higher Reynolds number (Re) and away from the wall, the streamwise component is severely underpredicted, as well as the transition in the mean velocity from the log to the wake profiles. In this area a significant change of behavior was observed in the DNS pressure-strain term, entirely ignored in the models.

1. Introduction

Second moment closures have the ability to account exactly for turbulence "production" terms due to shear, rotation and stratification, and to provide a better description than eddy viscosity models of the Reynolds stresses—a corner stone for complex flows involving heat transfer, two-phase flows, or combustion. However they are mainly used by industry in their high Re form, since near-wall models are both unsatisfactory and rather difficult to solve numerically.

Since the publication of the budgets of the Reynolds stresses in a channel flow by Mansour, Kim & Moin (1988), a variety of near-wall second moment closures have been proposed (see review of 9 models by So *et al.*, 1990). Some of them were more or less successful, but they are very seldom used outside low Reynolds number channel flows. Most of them use damping functions to force homogeneous models to comply with near wall turbulence features. A sound general principle is to avoid explicit use of the distance to the wall; however, this tends to render the models

1 EDF/DER/LNH, 6 quai Watier, 78400 Chatou, France

2 Center for Turbulence Research

rather difficult to converge numerically since the damping functions then depend on parameters of the unknown solution (such as the turbulent Reynolds number $k^2/\varepsilon\nu$). Launder & Tselepidakis (1991), for instance, did a careful term by term fit to each component of the Reynolds stress balance obtained by DNS, but the overall model proved somewhat unstable especially when gravitational damping was added (Laurence, 1993).

A common feature of these models is that all the terms (except diffusion) are related algebraically to the local values of the solution. Such local representation is in contradiction to the very large structures (hundreds of wall units) interacting with the wall and inhomogeneity of the velocity profile.

In contrast to this previous approach, Durbin (1993) was able to reproduce quite satisfactorily the features of near-wall flows by combining the very simple 'IP' homogeneous second moment closure (Launder, Reece & Rodi, 1975) with a nonlocal (elliptic) approach representing the wall blocking effect on the large eddies. The present study was aimed at a closer comparison of the elliptic operator with DNS budgets and an analysis of what could be gained by combining it with a more sophisticated second moment closure (SMC).

The Craft-Launder (1991) cubic SMC, either in free flows or in combination with wall functions or a low Re two-equation model, was shown to give better predictions than the IP model in a variety of flows (round and plane jets, impinging jets, tube bundles, swirling jets). A characteristic of near wall flows (also present in shear flows) is the strong reduction of the normal stress compared to the spanwise and longitudinal stresses. The Launder-Craft cubic model reproduces this effect in free flows and to some extent in the log-layer of a channel flow (Launder and Tselepidakis, 1991). Lee, Kim & Moin (1990) showed that many features of wall flows are also present in high shear homogeneous flows, though not accounting totally for the very high anisotropies in a near wall flow. Thus, our project was motivated by the idea that by combining the cubic model with the elliptic operator, to correctly acknowledge what is due to the high shear and what is due to the wall blocking effect, an improved model would result.

2. Elliptic relaxation

Following the procedure developed by Durbin (1993) the Reynolds-stress transport equation is written as:

$$D_t \overline{u_i u_j} = P_{ij} + \varphi_{ij} - \overline{u_i u_j} \frac{\varepsilon}{k} + T_{ij} + \nu \nabla^2 \overline{u_i u_j} \quad (1)$$

$$\begin{aligned} P_{ij} &= -\overline{u_i u_k} \partial_k U_j - \overline{u_j u_k} \partial_k U_i \\ \varphi_{ij} &= -\overline{u_i \partial_j p} - \overline{u_j \partial_i p} - \varepsilon_{ij} + \overline{u_i u_j} \frac{\varepsilon}{k} \\ T_{ij} &= -\partial_k \overline{u_k u_i u_j} \end{aligned} \quad (2)$$

The term φ_{ij} differs from the usual pressure-strain ϕ_{ij} since it includes the misalignment of the dissipation tensor and the Reynolds stress tensor:

$$\varphi_{ij} = \phi_{ij} - \left(\varepsilon_{ij} - \overline{u_i u_j} \frac{\varepsilon}{k} \right). \quad (3)$$

This unclosed term, called hereafter 'relaxed pressure-strain', is obtained by solving an elliptic equation:

$$L^2 \nabla^2 \frac{\varphi_{ij}}{k} = \frac{\varphi_{ij} - \varphi_{ij}^h}{k}. \quad (4)$$

For homogeneous turbulence φ_{ij} in Eq. 4 reduces to φ_{ij}^h , for which any standard redistribution model ϕ_{ij}^h can be used:

$$\varphi_{ij}^h = \phi_{ij}^h + \text{dev}(\overline{u_i u_j}) \frac{\varepsilon}{k}, \quad (5)$$

where 'dev' is the deviatoric operator:

$$\text{dev}(\overline{u_i u_j}) = \overline{u_i u_j} - \overline{u_k u_k} \delta_{ij} / 3$$

The simple 'IP' model uses the Rotta return to isotropy and the 'isotropization of production'; i.e., the slow and rapid parts are modeled as:

$$\begin{aligned} \phi_{ij}^h &= \phi_{ij, \text{slow}} + \phi_{ij, \text{rapid}} \\ &= -C_1 \text{dev}(\overline{u_i u_j}) \frac{\varepsilon}{k} - C_2 \text{dev}(P_{ij}) \end{aligned} \quad (6)$$

Durbin(1993) applied elliptic relaxation to the IP model with the following modifications which define what is called hereafter the 'R-linear model':

$$\varphi_{ij}^h = -(C_1 - 1) \frac{\text{dev}(\overline{u_i u_j})}{T} - C_2 \text{dev}(P_{ij}) \quad (7)$$

where the time scale is defined as:

$$T = \max \left[\frac{k}{\varepsilon}, 6 \left(\frac{\nu}{\varepsilon} \right)^{1/2} \right]. \quad (8)$$

This time scale is also used in the dissipation equation in place of ε/k , preventing a singularity at the wall. The length scale L appearing in (4) is also prevented from going to zero at the wall using again a Kolmogoroff scale as a lower bound:

$$L = C_L \max \left[\frac{k^{3/2}}{\varepsilon}, C_\eta \left(\frac{\nu^3}{\varepsilon} \right)^{1/4} \right]. \quad (9)$$

Furthermore Eq. 4 is solved numerically by introducing an intermediate variable $f_{ij} = \varphi_{ij}/k$, and boundary conditions at the wall are imposed on the coupled $\overline{u_i u_j} - f_{ij}$ equations.

Last, the Daly-Harlow expression for the turbulent diffusion was used to model T_{ij} :

$$T_{ij} = \partial_l \left(C_\mu \frac{\overline{u_l u_m} T}{\sigma_k} \partial_m \overline{u_i u_j} \right) \quad (10)$$

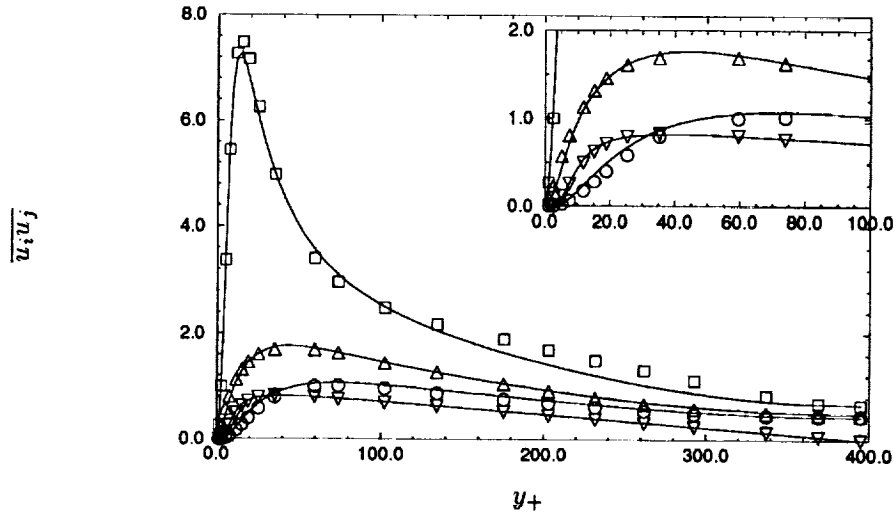


FIGURE 1. Reynolds Stresses, R-cubic model; \square , $\overline{u_1^2}$; \circ , $\overline{u_2^2}$; \triangle , $\overline{u_3^2}$; ∇ , $\overline{u_1 u_2}$.

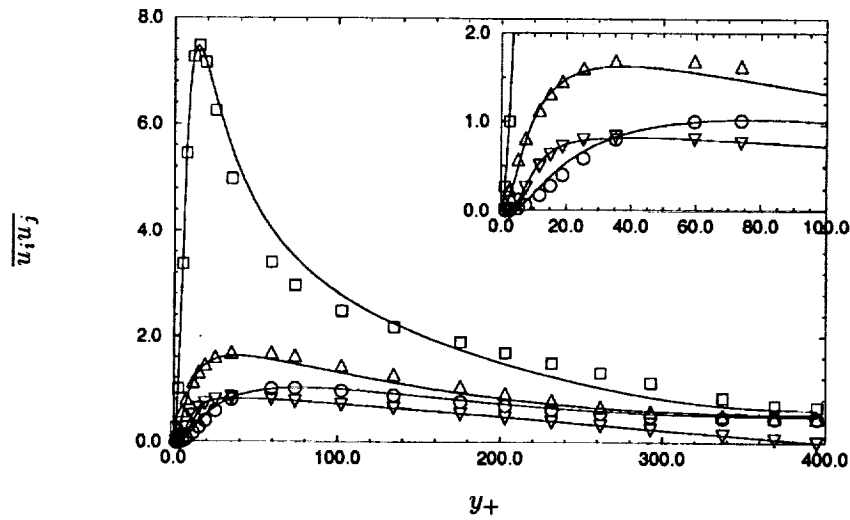


FIGURE 2. Reynolds Stresses, R-linear model. Symbols as in fig. 1.

3. Cubic order pressure-strain model

Defining the anisotropy tensor and its invariants as:

$$a_{ij} = \text{dev}(\overline{u_i u_j})/k, \quad A_2 = a_{ij}a_{ij}, \quad A_3 = a_{ij}a_{jk}a_{ki}, \quad A = 1 - 9/8(A_2 - A_3), \quad (11)$$

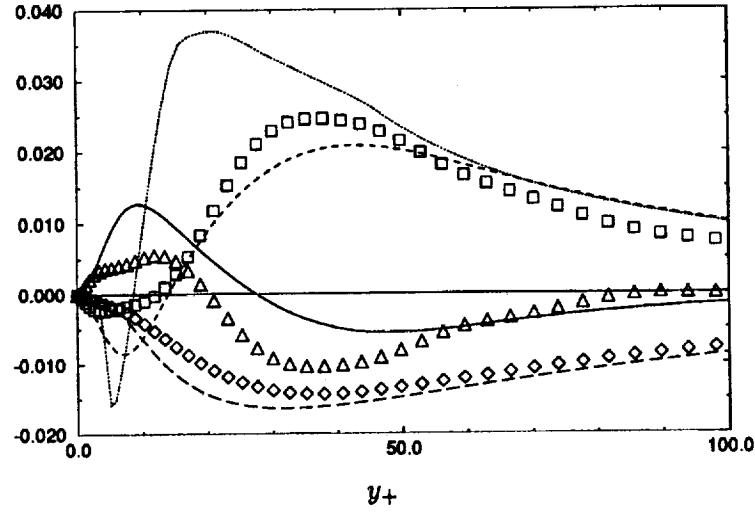


FIGURE 3. Balance terms of $\overline{u_2'^2}$; lines, R-cubic model; symbols, DNS; , φ_{22}^h ; ---- \square , φ_{22} ; — \triangle , total diffusion; --- \diamond , dissipation.

the cubic pressure-strain model of Craft & Launder (1991) is written as:

$$\begin{aligned} \phi_{ij}^{rapid} = & -0.6 \text{dev}(P_{ij}) + 0.3 a_{ij} P_{kk} \\ & - 0.2 \left(\frac{\overline{u_k u_j} \overline{u_l u_i}}{k} (\partial_l U_k + \partial_k U_l) - \frac{\overline{u_l u_k}}{k} (\overline{u_i u_k} \partial_l U_j + \overline{u_j u_k} \partial_l U_i) \right) \\ & - r (A_2 (P_{ij} - D_{ij}) + 3 a_{mi} a_{nj} (P_{mn} - D_{mn})) \end{aligned} \quad (12)$$

where: $D_{ij} = \overline{u_i u_k} \partial_j U_k - \overline{u_j u_k} \partial_i U_k$ and

$$\begin{aligned} \phi_{ij}^{slow} = & -(C_1 + 1) a_{ij} \varepsilon \\ & - C'_1 C_1 \text{dev}(a_{ik} a_{kj}) \varepsilon \end{aligned} \quad (13)$$

Thus the R-cubic model is defined with the following expression for φ_{ij}^h on the RHS of (4):

$$\varphi_{ij}^h = -C_1 (a_{ij} + C'_1 \text{dev}(a_{ik} a_{kj})) \frac{k}{T} + \phi_{ij}^{rapid} \quad (14)$$

With the values:

$$C_1 = 3.1 [A \min(A_2, 0.6)]^{1/2}, \quad C'_1 = 1.2, \quad r = 0.6$$

4. Low-Reynolds number channel flow

Figs. 1 & 2 show the Reynolds stresses compared to the DNS data at $Re=395$ (unpublished CTR simulation), as obtained by the relaxed cubic model and the relaxed IP model, respectively. The $\overline{u_3'^2}$ component is slightly too close to the $\overline{u_2'^2}$ component with the IP model. Both models predict a too steep decrease of $\overline{u_1'^2}$ away from the wall.

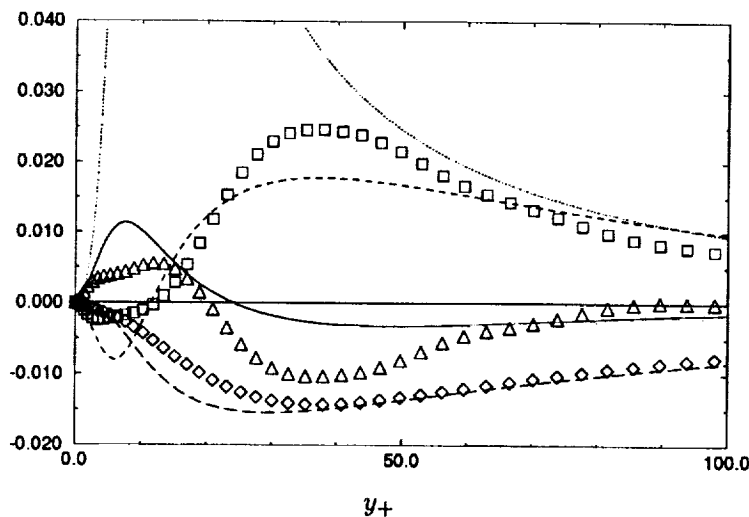


FIGURE 4. Balance terms of $\overline{u_2^2}$, R-linear model; captions as in Fig. 3.

The budgets of the normal stress $\overline{u_2^2}$ are given in Figs. 3 and 4 for the R-cubic and R-linear models respectively. The dotted lines are the source term ϕ_{ij}^h in Eq. 4; the dashed line is the solution to Eq. 4 and provides the relaxed pressure-strain that enters the solutions shown in Figs. 2 and 3. Note that by $y^+ \approx 80$, ϕ_{ij} has relaxed to ϕ_{ij}^h . Figs. 3 and 4 are plotted on the same scale to show that the relaxed pressure-strain terms are nearly identical even though the maximum of ϕ_{22} at $y^+ = 20$ in the homogeneous IP model is well out of range (0.11 in Fig. 4; i.e., 3 times that of the cubic model). This demonstrates that the solution to the relaxation equation has a large contribution coming through the boundary conditions. This blocking effect gives adequate near-wall behavior despite serious inaccuracies of the homogeneous model on the r.h.s of Eq. 4. The agreement with the balance terms obtained from DNS is satisfactory. For this comparison the DNS data were processed as in Eq. 1, in which T_{ij} and $\nu \nabla^2 \overline{u_i u_j}$ are combined as total diffusion. Note that differences between the ϕ_{22} term and the corresponding DNS data are compensating for visible defects in the diffusion model, Eq. 10. Since the $\overline{u_2^2}$ profile was seen to be quite accurately predicted, the Daly Harlow model of turbulent diffusion needs to be revisited.

Previous experience with the standard Launder-Tselepidakis model exhibited difficulties in solving the $\overline{u_2^2}$ balance because the normal stress component goes to zero as y^4 at the wall, while its balance terms remain large. In the form of Eq. 1, pressure strain now balances most of the diffusion while the remaining dissipation is a small, numerically stabilizing term. As $y_+ \rightarrow 0$, the molecular diffusion balances the relaxed pressure-strain $\phi_{22} \equiv k f_{22}$, both of them going to zero, which is precisely the boundary condition imposed on the coupled system $u_2^2 - f_{22}$.

A slightly less satisfactory agreement is obtained for the budget of $\overline{u_1 u_2}$ shown in Fig. 5. The small overestimation of the normal stress seen in Fig. 1 results in

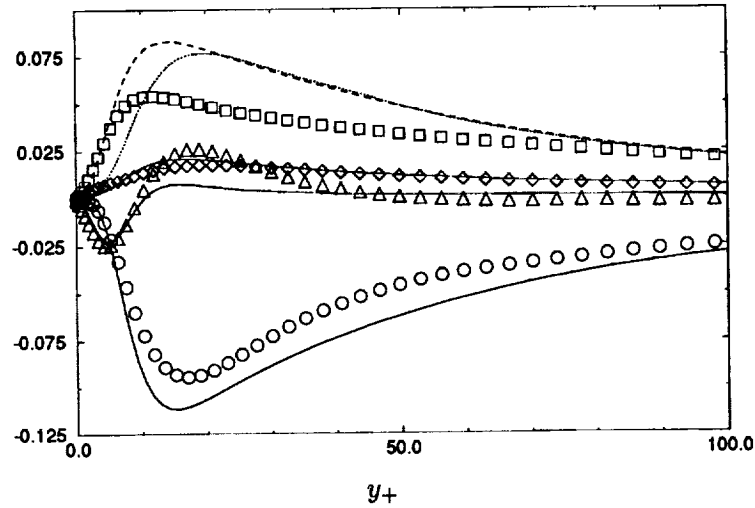


FIGURE 5. Balance terms of $\overline{u_1 u_2}$; lines, R-cubic model; symbols, DNS.; — \circ , production; \circ , ρ_{12}^h ; ---- \square , ρ_{12} ; — \triangle , total diffusion; ---- \diamond , dissipation.

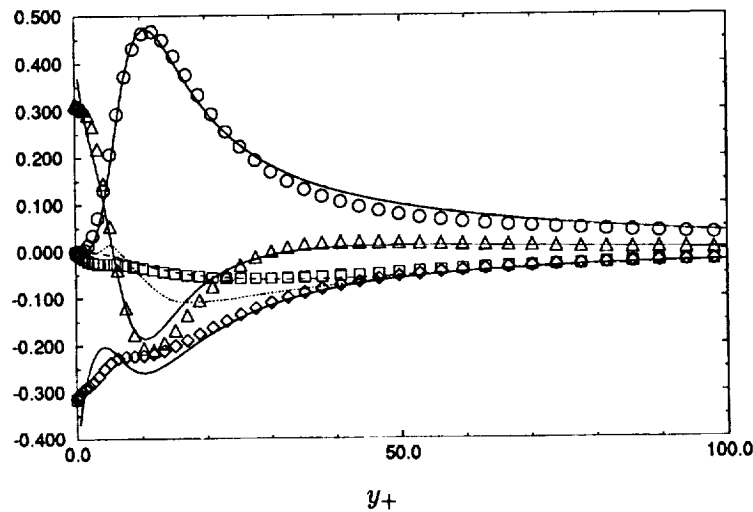


FIGURE 6. Balance terms of $\overline{u_1^2}$, R-cubic model; captions as Fig. 5.

a visible overprediction of the production in the near wall layer, compensated by a similar overprediction of the pressure-strain. Since the extent of agreement for the latter is quite different depending on which component is examined, further improvement could only be obtained by a tensorial correction whereas only global coefficient tuning was undertaken here.

Fig. 6 shows the balance of the streamwise stress $\overline{u_1^2}$. The production term becomes dominant and the pressure-strain is now a small part of the budget. The dissipation is quite well predicted. The ϵ model equation is only changed from its

standard high Re form by the use of T in place of k/ε (Durbin, 1993). The production of dissipation needs to be slightly increased very near the wall. Hanjalic & Launder (1976) introduced an extra production term, proportional to the second derivative of the mean velocity; but Rodi & Mansour (1990) showed that such a term was too strong below $y_+ = 10$. In the R-linear model production is enhanced by modifying the production constant $c_{\varepsilon 1}$ as:

$$c'_{\varepsilon 1} = c_{\varepsilon 1} + a_1 \frac{P}{\varepsilon} \quad (15)$$

with $a_1 \approx 0.1$. The dissipation equation is then:

$$D_t \varepsilon = \frac{c'_{\varepsilon 1} \frac{1}{2} P_{kk} - c_{\varepsilon 2} \varepsilon}{T} + \partial_k \left(\left(\nu + \frac{C_\mu \overline{u_k u_l} T}{\sigma_\varepsilon} \right) \partial_l \varepsilon \right) \quad (16)$$

A dependence on A_2 was added in the present R-cubic model to make sure the modification would have no effect on free shear flows, since A_2 only attains values near unity in the buffer layer where the turbulence becomes highly anisotropic:

$$c'_{\varepsilon 1} = c_{\varepsilon 1} (1 + a_1 \min(A_2, 1)^2 \frac{P}{\varepsilon}) \quad (17)$$

The kink in ε_{11} near $y_+ = 10$ is exaggerated but again compensates for a defect in the diffusion model. Note that in (16) no damping function is needed before $c_{\varepsilon 2}$ since $\frac{\varepsilon^2}{k}$ has been replaced by $\frac{\varepsilon}{T}$ which is finite.

The distribution of the various structure parameters used throughout the paper are given in Fig. 7. The A_2 parameter becomes very large below $y_+ = 30$, characterizing nearly 2-D turbulence and providing a means of isolating the transition layer, whereas the ratio of production over dissipation reaches values of about 1.5, which can also be found in free shear flows. The Rotta constant C_1 from the Launder-Craft model goes to zero at the wall, indicating that one might need a smaller elliptic correction than the linear IP model. The difference $c_{\varepsilon 2} - c_{\varepsilon 1}$ which can be related to the von Karman constant is seen to be fairly constant in the log-layer.

We consider in Fig. 8 the split of ϕ_{22} into the slow part and the rapid part modeled by Eq. 12. The slow part (to which the quadratic component (s_2) makes a small contribution) is dominating the rapid part and is acting 'naturally' to reduce the isotropy. The rapid part is determined largely by the linear term (the first term on the r.h.s. of Eq. 12, which is referred to as r_1 in figure 8) since the second and third terms (r_2 and r_3) seem to cancel each other. However, the model does not reduce to the linear contributions to the slow and rapid part (s_1 and r_1) (which is just the IP model) because r_3 takes a positive ('natural') sign in the spanwise stress budget. Also, in the shear stress budget r_2 is now acting 'anti-naturally' and r_3 'naturally', as can be seen in Fig. 9.

Fig. 10 shows the velocity profile from the $Re_\tau = 395$ DNS and the Comte-Bellot (1965) experiment at $Re_\tau = 2420$ ($Re = 57,000$). The latter when matched with the standard log-law, $U^+ = 1/\kappa \log(y_+) + C$, gives an additive constant of $C=7$,

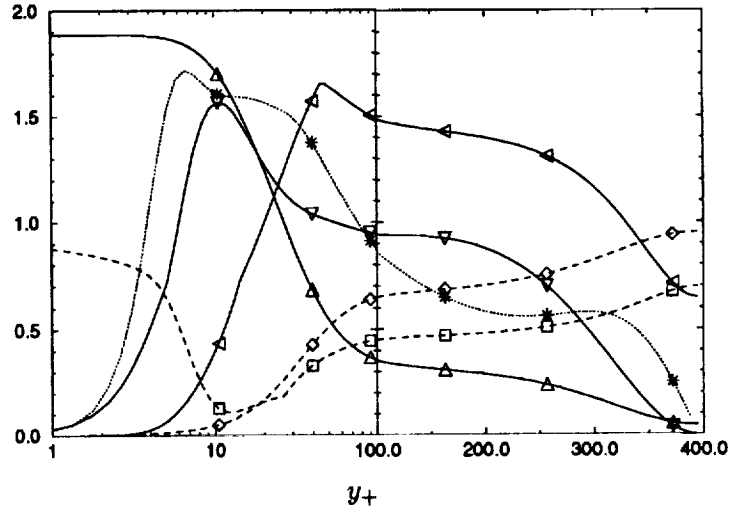


FIGURE 7. Structure parameters; see Eqs. 11 and 14. \square , $ce_2 - ce_1$; \diamond , A ; \triangle , A_2 ; ∇ , C_1 ; ∇ , P/ε ; $*$, dl/dy .

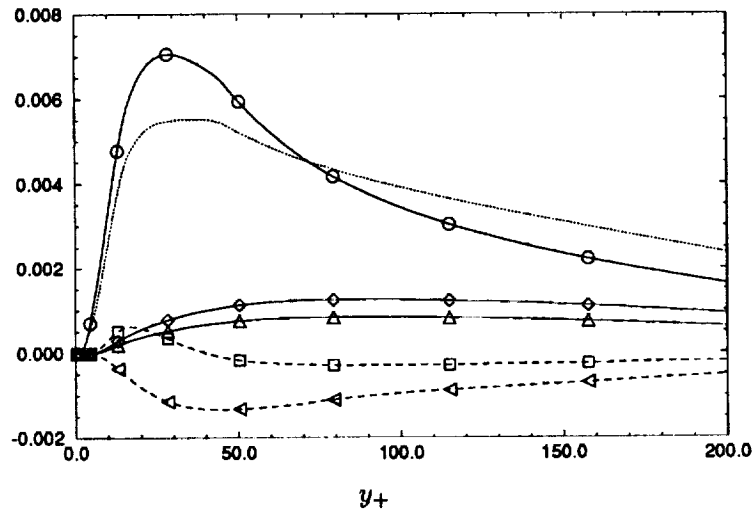


FIGURE 8. Split of ϕ_{22} in the cubic model. \circ , s_1 ; \square , s_2 ; \diamond , r_1 ; \triangle , r_2 ; ∇ , r_3 ; , total.

which is unusually high but will serve here to emphasize the effect of C_L in Eq. 9. Models are usually calibrated to yield $C=5.5$ and $\kappa=.41$ (dot-dashed line). The constant C is known to have a Reynolds dependence and is related to the Van Driest damping factor A^+ ; i.e., it depends on the rate at which the shear stress increases in the transition in the region $10 < y_+ < 30$, effectively accelerating the mean flow. This also introduces a pressure-gradient dependence.

With the R-cubic model described up to now, a best fit with the log-profile was

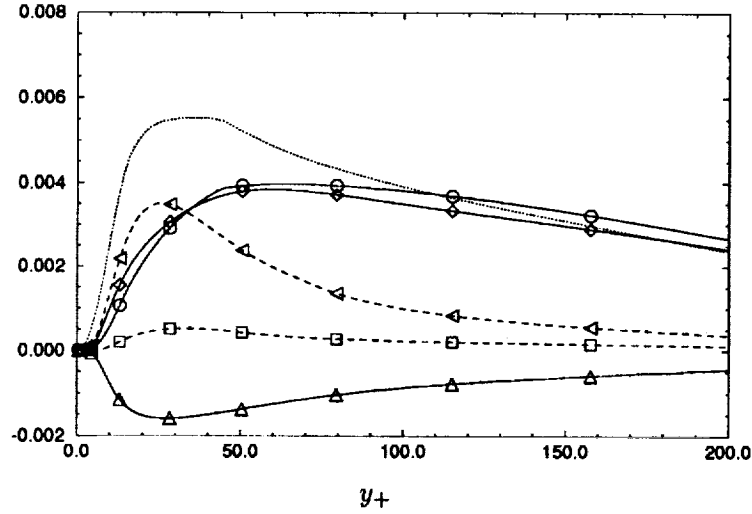


FIGURE 9. Split of ϕ_{12} in the cubic model. Symbols as in fig. 8.

obtained with $C_L = 0.25$. The homogeneous version of the cubic pressure-strain model yields an overestimation of the slope of the velocity profile. Thus Launder-Tselepidakis included a Gibson-Launder type of wall reflection (Eq. 24) to reduce the pressure-strain return to isotropy. Alternatively, they introduced an effective velocity gradient in the pressure strain model defined as:

$$\nabla U_i^{eff} = \nabla U_i + c^{eff} l (\nabla l \cdot \nabla) \nabla (U_i), \quad l = \frac{k^{1/2} \overline{u_n u_n}}{\varepsilon} \quad (18)$$

In the present 1-D problem, this is equivalent to:

$$\frac{\partial U^{eff}}{\partial y} = \frac{\partial U}{\partial y} + c^{eff} l \frac{\partial l}{\partial y} \frac{\partial^2 U}{\partial y^2} \quad (19)$$

Or, since $\phi_{ij,r}$ is linear in the mean shear:

$$\phi_{ij,r}^{eff} = \phi_{ij,r} + c^{eff} l \frac{\partial l}{\partial y} \frac{\partial \phi_{ij}^r}{\partial y} \quad (20)$$

In the log-layer ϕ behaves as y^{-1} so the effect is to reduce ϕ_{ij} by a factor which can be estimated using standard log-law assumptions as about 40%.

Note that this non-local effect could be incorporated in the relaxation operator by replacing $k L^2 \nabla^2 \frac{\rho_{ij}}{k}$ in (4) by:

$$\nabla \cdot (L^2 \nabla \frac{\rho_{ij}}{k}) = L^2 \nabla^2 \frac{\rho_{ij}}{k} + 2L \nabla(L) \nabla \frac{\rho_{ij}}{k} \quad (21)$$

In the log region, if we assume $\rho_{ij} = \phi_{ij}$, and neglect the effect of variations of k , the first term on the RHS has the same sign as ρ_{ij} thus increasing the return to

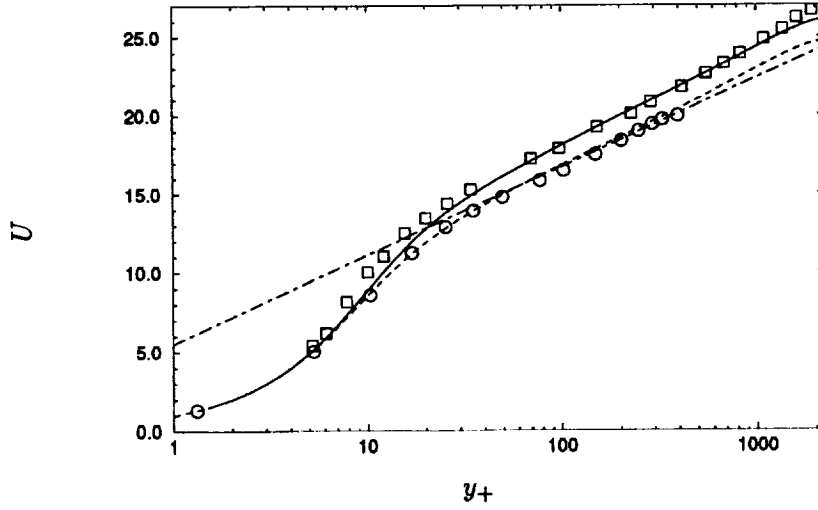


FIGURE 10. Velocity profiles, R-cubic model. ----, $c_1^{eff} = 0.12$, $c_2^{eff} = 0.1$, $cl = 0.15$; —, $c_1^{eff} = 0.12$, $c_2^{eff} = 0.1$, $cl = 0.22$; - · -, $U^+ = 1/\kappa \log(y_+) + C$; o, DNS; □, Comte-Bellot

isotropy (observed if Fig. 4 is plotted for $y_+ > 100$) while the second term actually reduces the return to isotropy, which is the effect sought by using wall echo terms.

This interesting idea, which avoids any explicit reference to the distance to the wall, was for the time being retained in a simpler version as follows:

$$\phi_{ij,r}^{eff} = \left(1 - \min \left[c_2^{eff} \left(\frac{\partial l}{\partial y} \right)^2, .3 \right] \right) \phi_{ij,r} \quad (22)$$

and

$$\phi_{ij,s}^{eff} = \left(1 - \min \left[c_1^{eff} \left(\frac{\partial l}{\partial y} \right)^2, .3 \right] \right) \phi_{ij,s} \quad (23)$$

The following combination:

$$c_1^{eff} = .12, c_2^{eff} = .1, C_L = .15$$

yielded the more satisfactory agreement, increasing U in the transition layer and slightly decreasing the slope of U further away from the wall in better agreement with the log-law as shown by the dashed curve in Fig. 10. The solid line obtained with $c_1^{eff} = .12$, $c_2^{eff} = .1$, $C_L = .22$ shows that in the present form, the relaxation effect is limited to the transition layer, whereas in the R-linear model used without Eqs. 22, 23, it also strongly affects the log-layer (Fig. 11).

The final form of the model at this stage and for which the results were shown in Figs. 1-10 is thus the standard Craft-Launder model, with the elliptic relaxation and the modifications in Eq. 22 and the values:

c_{ϵ_1}	c_{ϵ_2}	c_μ	σ_ϵ	σ_k	C_L	C_η	a_1	c_1^{eff}	c_2^{eff}
1.	f(A, A ₂)	.23	1.3	1.	.15	80.	.2	.12	.1

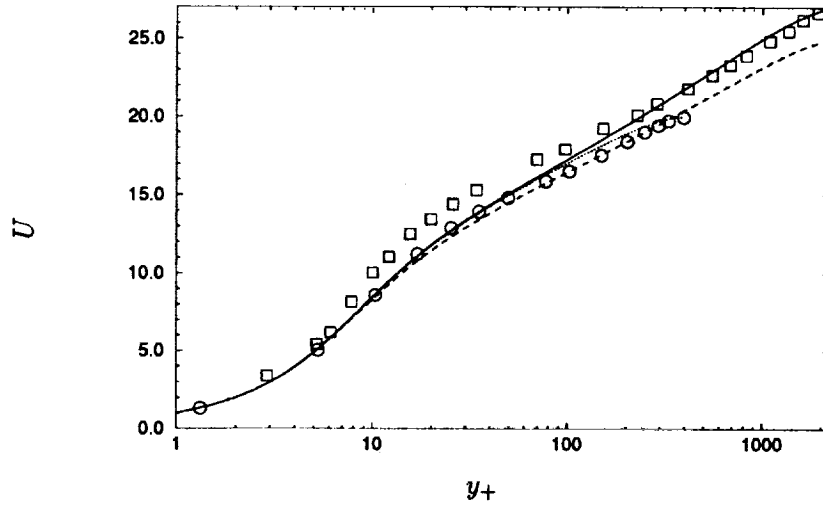


FIGURE 11. Mean velocity profiles, R-linear model. For captions see Fig. 10

while for the R-linear model used here the constants of Durbin (1993) were used:

c_{ϵ_1}	c_{ϵ_2}	C_μ	σ_ϵ	σ_k	C_L	C_η	a_1	C_1	C_2
1.44	1.9	.23	1.65	1.2	.2	80.	.1	1.22	0.6

Note that the pressure strain constant C_1 is lower than the standard value; this reduction could be avoided by using the gradient of the length scale as an inhomogeneity indicator. Also the following Gibson-Launder formulation,

$$\phi_{ij}^w = \phi_{kln} n_k n_l \delta_{ij} - 3/2 \phi_{ik} n_k n_j - 3/2 \phi_{jk} n_k n_i, \quad (24)$$

was not used with the Craft-Launder model since $\overline{u_2^2}$ is sufficiently suppressed by the rapid term of the cubic model.

At $Re=395$, Fig. 12 shows that the R-linear and R-cubic predictions are almost undistinguishable. The fact that all models known to the authors seem to underpredict the increase in velocity in the central part of the channel (the wake region) where they recover their homogeneous form is somewhat puzzling. The centerline velocity (and more importantly, the skin friction in boundary layers) seems to be recovered only at the expense of predicting a somewhat lower von Karman constant.

Considering the $\overline{u_1 u_2}$ balance equation, neglecting diffusion and dissipation,

$$0 = -\overline{u_2^2} \frac{\partial U}{\partial y} + \phi_{12}, \quad (25)$$

one sees that with $\overline{u_2^2}$ constant, the magnitude of the velocity gradient is allowed to increase (relative to y^{-1} in the log layer) only if the pressure strain decreases less than y^{-1} . This is indeed the behavior of exhibited by the DNS data (Fig. 13)

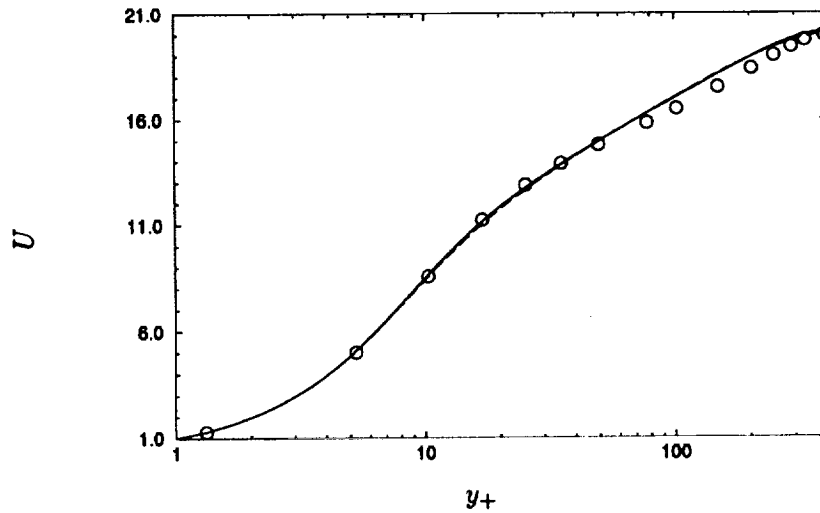


FIGURE 12. Velocity at $Re=395$: —, R-cubic; ----, R-linear. For captions see Fig. 10.

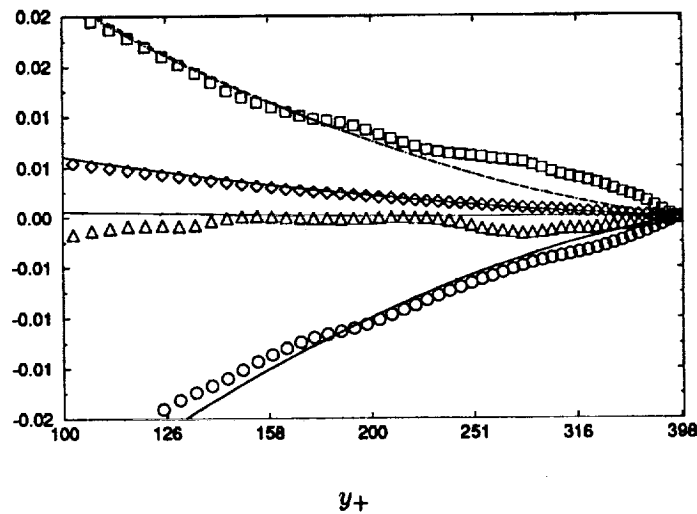


FIGURE 13. Budget of terms in the $\overline{u^2}$ equation near channel centerline, captions as Fig. 4.

and seems to be ignored by the models. In fact the relative increase of the pressure strain exceeds that of the production and is balanced by pressure diffusion. A similar behavior was found for all Reynolds-stress budgets.

With the present gradient transport assumption, a zero value is predicted for the total diffusion (pressure + turbulent) since $\overline{u_1 u_2}$ is linear, but non-zero pressure diffusion might be accounted for by the non-local formulation investigated by Demuren *et al.* in the present volume.

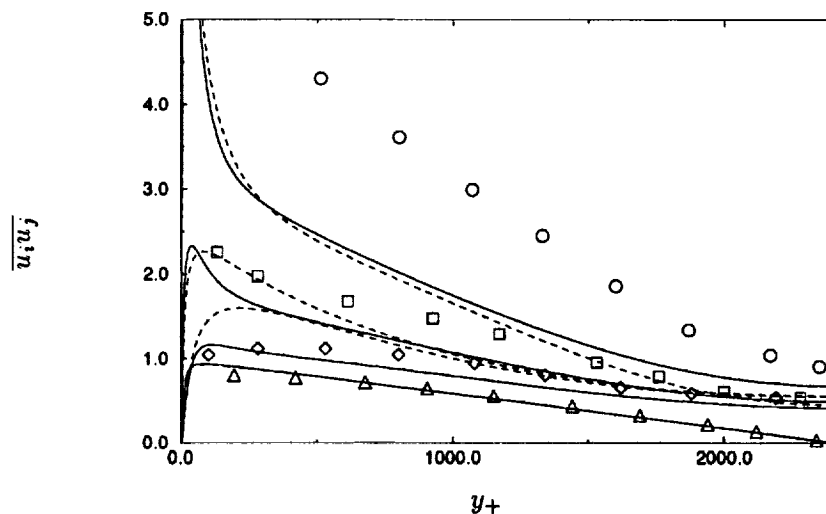


FIGURE 14. Reynolds stresses for the channel flow at $Re=57,000$. \circ , $\overline{u_1^2}$; \diamond , $\overline{u_2^2}$; \square , $\overline{u_3^2}$; \triangle , $\overline{u_1 u_2}$. —, R-cubic; ----, R-linear.

Fig. 14 compares the Reynolds-stress distributions throughout the channel at high Reynolds number (Comte-Bellot experiment $Re = 57,000$). One major drawback is that $\overline{u_1^2}$ is severely underestimated. Experiments show an extension with Re of the plateau region of the stress maxima (Antonia *et al.*, 1992), whereas the models follow this trend more moderately. This is a generic problem since the standard high Re Gibson-Launder model with wall functions yields similar underestimations away from the wall. One sees, however, that the R-cubic model reproduces a better separation between normal and spanwise components than the R-linear model for which this separation is limited to the log layer.

5. Other calculations

The skin friction was computed for a zero pressure gradient, boundary layer. The R-cubic model overpredicts C_f , which is related to the difficulty in predicting the wake region in the centerline of channel flow that was observed previously (Fig. 10).

The R-cubic model was also tested on the flow over a backward facing step but without Eqs. 22-23 and yielded similar, if not less satisfactory, predictions in comparison to the R-linear model used by Ko & Durbin (1993).

Conclusion

The present study used the DNS results of a channel flow at $Re_\tau = 395$ to confirm that homogeneous, second moment closures can be quite easily made to comply with near-wall turbulence characteristics by applying the elliptic relaxation procedure of Durbin (1993). Physically, it models the blocking effect that the wall imposes on the the fluctuating pressure, thus alleviating the need for Re dependent 'damping functions'.

It was found that the standard relaxation model produces a reduction of 'return to isotropy' in the near wall layer ($y_+ < 80$). This effect is essentially due to the boundary conditions. In this region, the elliptic relaxation is so strong that the switch from a linear to a cubic pressure strain model had a nearly unnoticeable effect on the budgets of the stresses. After imposing the elliptic relaxation these budgets compare very well with the DNS data. An urgently needed improvement concerns the Daly-Harlow turbulent diffusion term which was not studied here.

Further away from the wall, it seems that the strong inhomogeneity of the log-layer has also a significant blocking effect, underestimated by the original elliptic relaxation combined with the simple IP second moment closure. Using the Craft & Launder model, the wall normal stress was better reproduced, but still insufficiently to avoid further inhomogeneity corrections. This is the reason that the Gibson & Launder 'wall echo' model was still required at significant distances from the wall. In the latter, reference to the distance to the wall can be avoided by using the gradient of the turbulence length scale as suggested by Launder & Tselepidakis, and which could be included along with elliptic relaxation.

Outside the log-layer, the DNS data show a significant change in the behavior of the pressure strain terms, which explains the increase of the velocity gradient, but is not reproduced by the models. The latter seem to compensate for this omission by overpredicting the slope in the log-layer. Near wall models are usually compared to DNS data at low Re , but for practical applications more attention should be given to higher Re flows, with the challenging feature that the profiles of the stresses show a strong Re dependence (i.e., they do not collapse on plots scaled in wall units). In particular the streamwise stress is severely underpredicted at high Re .

REFERENCES

- ANTONIA, R. A., TEITEL, M., KIM, J., & BROWNE, L. W. B. 1992 Low-Reynolds-number effects in a fully developed turbulent channel flow. *J. Fluid Mech.* **236**, 579-605.
- COMTE-BELLOT, G. 1965 Ecoulement turbulent entre deux parois paralleles. *Pub. Scien. et Tech. du ministere de l'air*.
- CRAFT, T. J., LAUNDER, B. E. 1991 Computation of impinging flows using second moment closures. *8th. Symp. on Turbulent Shear Flows, T. U. Munich*. 8-5.
- DURBIN, P. 1991 Near wall second moment closures without 'damping functions'. *Theoret. Comp. Fluid Dyn.* **159**, 105.
- DURBIN, P. 1993 A Reynolds-stress model for near-wall turbulence. *J. Fluid Mech.* **249**, 465-498.
- GIBSON, M. M., & LAUNDER, B. E. 1978 Ground effects on pressure fluctuations in the atmospheric boundary layer. *J. Fluid Mech.* **86**, 491-511.
- KO S., & DURBIN, P. 1993 Application of a near-wall turbulence model to adverse pressure gradient and separating boundary layers. *Proc. Int. Conf. on Near-Wall Turbulent Flows*. 145-154.

- LAUNDER, B. E., REECE, G. J., & RODI, W. 1975 Progress in the development of a Reynolds-stress closure. *J. Fluid Mech.* **68**, 537-566.
- LAUNDER, B. E., TSELEPAKIS, D. P. 1991 Progress and Paradoxes in Modeling Near-Wall Turbulence. *8th. Symp. on Turbulent Shear Flows, T. U. Munich.* 29-15.
- LAURENCE, D., MAUPU, V., GALLAND, J. C., & TEISSON, C. 1993 A sediment laden open channel flow simulation with recent Reynolds-stress-flux transport models. *Eng. Turb. Model. and Exp* Rodi, Martelli Eds., Elsevier. 73-82.
- LEE, M. J., KIM, J., & MOIN, P. 1990 Structure of turbulence at high shear rate. *J. Fluid Mech.* **216**, 561-498.
- MANSOUR, N. N., KIM, J., & MOIN, P. 1988 Reynolds-Stress and Dissipation-rate budgets in a turbulent channel flow. *J. Fluid Mech.* **194**, 15-44.
- RODI, W., & MANSOUR, N. N. 1990 One equation near-wall turbulence modeling with the aid of direct simulation data. *Proc. 1990 Summer Program.* Center for Turbulence Research, NASA Ames/Stanford Univ. 107-124.
- SO, R. M. C., LAI, Y. G., ZHANG H. S., & HWANG B. C. 1991 Second order near-wall turbulence closures: a review. *AIAA J.* **29-11**, 1819-1835